

**SILICOALUMINOPHOSPHATES NUMBER 5 (SAPO-5)  
ZEOLITE TEMPLATED BY IMIDAZOLIUM  
COMPOUNDS AS CATALYST FOR FRIEDEL-CRAFTS  
ACYLATION OF 2-METHYLFURAN**

**ISMAIL ALHASSAN AUWAL**

**UNIVERSITI SAINS MALAYSIA**

**2021**

**SILICOALUMINOPHOSPHATES NUMBER 5 (SAPO-5)  
ZEOLITE TEMPLATED BY IMIDAZOLIUM  
COMPOUNDS AS CATALYST FOR FRIEDEL-CRAFTS  
ACYLATION OF 2-METHYLFURAN**

by

**ISMAIL ALHASSAN AUWAL**

**Thesis submitted in fulfilment of the requirement  
for the degree of  
Doctor of Philosophy**

**March 2021**

## ACKNOWLEDGEMENT

All the praises and thanks be to Allah, who spare my life to witness this great moment.

I will like to first thank my parents. The unconditional love and support of my mother, Hajia Rahma Sulaiman, and my father, Mallam Alhassan Auwal, have made me the person I am today. They taught me the morals and values of life that made me understand the importance of education. Their sacrifices and encouragement had helped me how to achieve my dreams.

I would like to express indebtedness to my wife, Umami Auwal, and our precious daughters, Rahma Ismail and Fatima Ismail, for their love and understanding during my PhD study. They have been my support and encouragement. I also want to thank my elder brother, Auwal Alhassan, my sisters, my other family members and friends. Their love, support and patience are sincerely appreciated.

A million thanks to Assoc. Prof. Dr. Ng Eng Poh who is a great advisor. I am very honored and privileged to be his student. His coaching technique is extremely effective, and I can proudly say that what I have learned from him is beyond research skills, rather he taught me discipline, punctuality and perseverance.

I would like to acknowledge Universiti Sains Malaysia, Nigerian Tertiary Education Trust Fund (TETFund) and research grants (RUI (1001/PKIMIA/8011128), USM Bridging Fund (304/PKIMIA/3616506) and FRGS (203/PKIMIA/6711642) for financial support and scholarships. My sincere thank also goes to my employer, Sule Lamido University Kafin Hausa, for approving my study leave. A special thank is also dedicated to all staff of the School of Chemical Sciences, USM. Lastly, my earnest gratitude goes to my current and former lab mates, Ms. Nurhidayahni, Mr. Ken, Dr. Tamara, Dr. Ghadah, Ms. Cythia and Dr. Haruna. Their huge support, guidance and encouragement toward this journey are well appreciated.

## TABLE OF CONTENTS

<b>ACKNOWLEDGEMENT</b> .....	<b>ii</b>
<b>TABLE OF CONTENTS</b> .....	<b>iii</b>
<b>LIST OF TABLES</b> .....	<b>viii</b>
<b>LIST OF FIGURES</b> .....	<b>ix</b>
<b>LIST OF SCHEMES</b> .....	<b>xvi</b>
<b>LIST OF SYMBOL AND NOMENCLATURE</b> .....	<b>xvii</b>
<b>LIST OF APPENDICES</b> .....	<b>xx</b>
<b>ABSTRAK</b> .....	<b>xxi</b>
<b>ABSTRACT</b> .....	<b>xxiii</b>
<b>CHAPTER 1 INTRODUCTION</b> .....	<b>1</b>
1.1 General Introduction .....	1
1.2 Research objectives.....	4
1.3 Thesis overview .....	5
<b>CHAPTER 2 LITERATURE REVIEW</b> .....	<b>8</b>
2.1 Microporous zeolites.....	8
2.1.1 Formation of zeolite .....	11
2.2 Aluminophosphate (AlPO- <i>n</i> ) and silicoaluminophosphate (SAPO- <i>n</i> ) zeotypes.....	12
2.2.1 Mechanism of Si isomorphous insertion.....	16
2.3 SAPO-5 microporous materials .....	19
2.3.1 Synthesis of SAPO-5 molecular sieves.....	21
2.3.1(a) Dry-gel conversion method .....	21
2.3.1(b) Microwave irradiation method .....	23
2.3.1(c) Hydrothermal synthesis .....	25
2.3.2 Factors affecting the formation of SAPO-5 molecular sieves .....	27
2.3.2(a) Effect of crystallization temperature and time .....	28

2.3.2(b)	Effect of source and molar concentration of starting materials .....	30
2.3.3	Applications of SAPO-5 molecular sieves.....	39
2.3.3(a)	SAPO-5 in adsorption and separation .....	39
2.3.3(b)	SAPO-5 in ion-exchange.....	41
2.3.3(c)	SAPO-5 in catalysis.....	42
2.4	Friedel-Crafts acylation .....	44
2.4.1	Friedel-Crafts acylation of 2-methylfuran with acetic anhydride.....	46
2.5	Catalytic limitations and modifications of SAPO-5 .....	49
<b>CHAPTER 3 MATERIALS AND EXPERIMENTAL METHODS .....</b>		<b>52</b>
3.1.	Introduction.....	52
3.2	Preparation of imidazolium-based structure-directing agents .....	53
3.2.1	Synthesis of 1-propyl-2,3-dimethyl-1H-imidazole-3-ium bromide, [pmIm]Br .....	53
3.2.2	Synthesis of 1-benzyl-2,3-dimethyl-1H-imidazole-3-ium chloride, [bzmIm]Cl.....	54
3.2.3	Synthesis of 3-(2,3-dihydroxypropyl)-1,2-dimethylimidazolium-4-methylbenzene sulfonate, [dhmIm]OTs .....	54
3.2.4	Preparation of [pmIm]OH, [bzmIm]OH and [dhmIm]OH SDA solutions .....	56
3.2.5	Synthesis of SAPO-5 .....	56
3.3	Parameter study of crystallization of SAPO-5.....	57
3.4	Synthesis of metal chlorides grafted SAPO-5 (MCl <sub>x</sub> /SAPO-5) catalysts.....	58
3.5	Characterization techniques .....	59
3.5.1	X-ray diffraction (XRD) analysis .....	59
3.5.2	Fourier transform infrared (FTIR) spectroscopy .....	62
3.5.3	Field emission scanning electron microscopy (FESEM).....	63
3.5.4	Energy dispersive X-ray (EDX) spectroscopy.....	64

3.5.5	CHNS/O elemental analysis .....	65
3.5.6	Nuclear magnetic resonance (NMR) spectroscopy.....	66
3.5.7	Nitrogen gas adsorption-desorption analysis .....	68
3.5.8	Thermogravimetric analysis.....	70
3.5.9	Pyridine adsorption analysis .....	71
3.5.10	Gas chromatography (GC) analysis .....	73
3.5.11	Gas chromatography-mass spectrometry (GC-MS).....	74
3.6	Catalytic acylation reaction study .....	75
3.6.1	Non-microwave heating.....	76
<b>CHAPTER 4 CRYSTALLIZATION AND MORPHOLOGICAL STUDY OF SAPO-5 TEMPLATED BY IMIDAZOLIUMS OF DIFFERENT FUNCTIONAL GROUPS.....</b>		<b>80</b>
4.1	Introduction.....	80
4.2	Results and discussion .....	81
4.2.1	Characterization of imidazolium SDAs .....	81
4.2.1(a)	Characterization of propyl-2,3-dimethyl-1H-imidazole-3-ium bromide, [pmIm]Br .....	81
4.2.1(b)	Characterization of 1-benzyl-2,3-dimethyl-1H-imidazole-3-ium chloride, [bzmIm]Cl.....	83
4.2.1(c)	Characterization of 3-(2,3-dihydroxypropyl)-1,2-dimethylimidazolium-4-methylbenzene sulfonate, [dhmIm]OTs .....	85
4.2.2	Characterization of SAPO-5 microporous solids.....	88
4.2.2(a)	XRD analysis.....	88
4.2.2(b)	Solid yield analysis.....	92
4.2.2(c)	FESEM analysis .....	93
4.2.2(d)	Elemental analysis .....	94
4.2.2(e)	TG/DTG measurements.....	95
4.2.2(f)	Surface and texture properties .....	99

4.3	Summary .....	101
<b>CHAPTER 5 STUDY OF SYNTHESIS PARAMETERS ON THE CRYSTALLIZATION OF SAPO-5..... 102</b>		
5.1	Introduction.....	102
5.2	Results and discussions.....	105
5.2.1	Effect of crystallization time.....	105
5.2.2	Effect of P <sub>2</sub> O <sub>5</sub> molar ratio .....	109
5.2.3	Effect of P <sub>2</sub> O <sub>5</sub> /[bzmIm] <sub>2</sub> O molar ratio.....	112
5.2.4	Effect of H <sub>2</sub> O content.....	115
5.2.5	Effect of SiO <sub>2</sub> molar ratio .....	118
5.2.6	Effect of temperature .....	121
5.3	Solid yield examination .....	124
5.4	Formation study of SAPO-5 crystals .....	125
5.5	Summary .....	128
<b>CHAPTER 6 METAL CHLORIDES GRAFTED ON SAPO-5 (MCLX/SAPO-5) AS REUSABLE AND SUPERIOR CATALYSTS FOR ACYLATION OF 2-METHYLFURAN UNDER NON-MICROWAVE INSTANT HEATING CONDITION ..... 130</b>		
6.1	Introduction.....	130
6.2	Results and Discussion .....	131
6.2.1	Characterization .....	131
6.2.2	Catalytic testing .....	143
6.2.2(a)	Friedel-Craft acylation of 2-methylfuran over MeCl <sub>x</sub> /SAPO-5 .....	143
6.2.2(b)	Effect of reaction time and temperature .....	143
6.2.2(c)	Effect of catalyst loading.....	148
6.2.2(d)	Effect of heating mode .....	149
6.2.2(e)	Catalytic comparative study .....	150
6.2.2(f)	Catalyst reusability test.....	151

6.3	Summary .....	153
<b>CHAPTER 7 CONCLUSION AND RECOMMENDATIONS.....</b>		<b>155</b>
7.1	Conclusion .....	155
7.2	Recommendation of future work .....	158
<b>REFERENCES.....</b>		<b>160</b>
<b>APPENDICES</b>		
<b>LIST OF PUBLICATIONS</b>		



## LIST OF TABLES

		<b>Page</b>
Table 2.1	Some AlPO-n/SAPO-n based molecular sieves .....	13
Table 2.2	Some reported heating conditions of AFI-type molecular sieves.....	29
Table 2.3	Friedel-Crafts acylation of furans with various acylating agents under different conditions using Lewis acid catalysts.....	48
Table 2.4	Catalytic activity of surface-modified SAPO-5 material.....	50
Table 4.1	Elemental composition of [pmIm]Br .....	82
Table 4.2	Elemental composition analysis of [bzmIm]Cl .....	84
Table 4.3	Elemental composition analysis of [dhmIm]OTs .....	87
Table 4.4	General information of imidazolium cations used in this study.....	89
Table 4.5	Chemical composition and physicochemical properties of SAPO-5 solids.....	95
Table 4.6	Thermogravimetry data of as-synthesized SAPO-5 solids. ....	99
Table 5.1	Summary of the study of synthesis effect using various initial hydrogel compositions by altering the individual synthesis parameter .....	104
Table 6.1	Chemical compositions of metal chlorides supported on SAPO-5.....	137
Table 6.2	Calculated molecular formulae and elemental ratios of metal chlorides supported on SAPO-5 [334].....	138
Table 6.3	Textural and surface properties of MCl <sub>x</sub> /SAPO-5 solids.....	140
Table 6.4	Surface acidity of MCl <sub>x</sub> /SAPO-5 measured using pyridine (Py) adsorption coupled with FTIR spectroscopy technique.....	142
Table 6.5	The effect of heating method on acylation of 2-methylfuran catalyzed by ZnCl <sub>x</sub> /SAPO-5.....	150

## LIST OF FIGURES

		<b>Page</b>
Figure 2.1	Illustration of the IUPAC classification of porous materials [57] .....	8
Figure 2.2	The formation for zeolite framework where MeOH is metal hydroxide of group I or II that provide the compensating cation $M^+$ [60].....	9
Figure 2.3	Building units of zeolites and the framework structures of zeolites [63].....	10
Figure 2.4	The types of secondary building units (SUBs) found in zeolitic frameworks [69].....	14
Figure 2.5	Arrangement of tetrahedra in zeolite, AIPO-n, and SAPO-n molecular sieves, where $Me^{\oplus}$ and $R^{\oplus}$ are counter cation and structure directing agent, respectively.....	16
Figure 2.6	General substitution mechanism of Si atom in AIPO-n molecular sieves.....	17
Figure 2.7	A 2D representation of various mechanisms of Si insertion in AIPO-n framework: (a) SM1: Si→Al substitution, (b) SM2: Si→P substitution, and (c) SM3: 2Si→P,Al substitution which further divides into (d) SM3: 2Si→P,Al (generation of island), (e) SM3: 4Si→2P,2Al (generation of line), and (f) SM3: 4Si→2P,2Al (generation of ring). The oxygen atoms are not shown for simplicity. ....	18
Figure 2.8	A typical SAPO-5 framework with AFI topology formed by the assembly of several second building units The CBUs present in the AFI structure are displayed in the top row, with the framework oxygens omitted for clarity. [83].....	19
Figure 2.9	SAPO-5 crystals synthesized using different Al sources: (a) aluminum isopropoxide and (b) pseudo boehmite [99], and those synthesized at different pH using aluminum isopropoxide as Al source: (c) pH 9 and (d) pH 7 [22]. ....	21
Figure 2.10	A setup for the synthesis of SAPO-5 using dry gel conversion method via (a) steam-assisted conversion (SAC) and (b) vapor phase transport (VPT) routes. ....	23

Figure 2.11	A diagrammatic illustration of a microwave instrument for the synthesis of microporous materials .....	24
Figure 2.12	A typical setup for hydrothermal synthesis of SAPO-5 molecular sieve .....	26
Figure 2.13	Some reported structure directing agents used to crystalized AFI phase zeotypes (AlPO-5 and SAPO-5) [22-25, 155] .....	34
Figure 2.14	Demonstration of selective separation of xylene isomers over SAPO-5 molecular sieve with linear pore channels. ....	40
Figure 3.1	Synthesis route of [pmIm]Br. ....	53
Figure 3.2	Synthesis pathway of [bzmIm]Cl. ....	54
Figure 3.3	Synthesis route of [dhmIm]OTs .....	56
Figure 3.4	Physical appearance of (a) SAPO-5, (b) CuCl <sub>x</sub> /SAPO-5, (c) CoCl <sub>x</sub> /SAPO-5, (d) SnCl <sub>x</sub> /SAPO-5, (e) FeCl <sub>x</sub> /SAPO-5 and (f) ZnCl <sub>x</sub> /SAPO-5. ....	59
Figure 3.5	Diffraction of X-ray from a set of crystal planes. Two incident rays reflect from two planes of a crystal. The difference in path lengths is indicated by the dashed line [240].....	61
Figure 3.7	A simple illustration of NMR spectroscopy instrument [259].....	68
Figure 3.8	(a) Types of adsorption-desorption isotherms and (b) types of hysteresis loops based on IUPAC classification [262].....	70
Figure 3.10	Schematic representation of a gas chromatography-mass spectrometer (GC-MS) .....	75
Figure 3.11	Illustration of a non-microwave heating reactor [55] .....	77
Figure 4.1	FT-IR spectrum of [pmIm]Br .....	81
Figure 4.2	<sup>1</sup> H NMR spectrum of [pmIm]Br .....	83
Figure 4.3	FT-IR spectrum of [bzmIm]Cl.....	84
Figure 4.4	<sup>1</sup> H NMR spectrum of [bzmIm]Cl .....	85
Figure 4.5	FT-IR spectrum of [dhmIm]OTs .....	86
Figure 4.6	<sup>1</sup> H NMR spectrum of [dhmIm]Ts.....	88

Figure 4.7	XRD patterns of (a) pmIm-n, (b) bzmIm-n and (c) dhmIm-n solids after various heating times, and (d) a plot of crystallinity versus respective crystallization heating time of pmIm-n, bzmIm-n and dhmIm-n samples. * shows the XRD diffraction peaks due to the periodic crystal-like arrangement of [pmIm] <sup>+</sup> molecules in the SAPO-5 micropores.....	90
Figure 4.8	Solid yield profiles of (a) pmIm-n, (b) bzmIm-n and (c) dhmIm-n samples.....	92
Figure 4.9	FESEM images of (a,b) pmIm-5, (c,d) bzmIm-10 and (e,f) dhmIm-2.5 SAPO-5 crystals under different magnifications.....	94
Figure 4.10	TGA-DTG profiles of as-synthesized (a) [pmIm] <sup>+</sup> , (b) [bzmIm] <sup>+</sup> and (c) [dhmIm] <sup>+</sup> molecules.....	96
Figure 4.11	TGA-DTG profiles of as-synthesized (a) pmIm-5, (b) bzmIm-10 and (c) dhmIm-2.5 SAPO-5. ....	98
Figure 4.12	Nitrogen gas adsorption and desorption isotherms of calcined (a) pmIm-5, (b) bzmIm-10 and (c) dhmIm-2.5 SAPO-5.....	100
Figure 5.1	XRD pattern of (a) SH1, (b) SH2, (c) SH3, (d) SH4 and (e) SH5 samples after heating at 150 °C for 2 h, 4 h, 8 h, 10 h and 14 h, respectively. The solid products were prepared with a molar composition of 1Al <sub>2</sub> O <sub>3</sub> :2.5P <sub>2</sub> O <sub>5</sub> :2.5[bzmIm] <sub>2</sub> O:180H <sub>2</sub> O:0.47SiO <sub>2</sub> . ....	105
Figure 5.2	FESEM of (a) SH1, (b) SH3, (c) SH4, and (d) SH5 samples after heating at 150 °C for 2 h, 8 h, 10 h, and 14 h, respectively. The solid products were prepared with a molar composition of 1Al <sub>2</sub> O <sub>3</sub> :2.5P <sub>2</sub> O <sub>5</sub> :2.5[bzmIm] <sub>2</sub> O:180H <sub>2</sub> O:0.47SiO <sub>2</sub> . ....	106
Figure 5.3	Particle size distribution of (a) SH1, (b) SH3, (c) SH4, and (d) SH5 samples after heating at 150 °C for 2 h, 8 h, 10 h, and 14 h, respectively. The solid products were prepared with a molar composition of 1Al <sub>2</sub> O <sub>3</sub> :2.5P <sub>2</sub> O <sub>5</sub> :2.5[bzmIm] <sub>2</sub> O:180H <sub>2</sub> O:0.47SiO <sub>2</sub> .....	108
Figure 5.4	XRD patterns of (a) SH4 (w = 2.5), (b) SH7 (w = 3.0) and (c) SH8 (w = 3.5) where the solid products were prepared with a molar composition of 1Al <sub>2</sub> O <sub>3</sub> :wP <sub>2</sub> O <sub>5</sub> :2.5[bzmIm] <sub>2</sub> O:180H <sub>2</sub> O:0.47SiO <sub>2</sub> heated at 150 °C for 10 h. The asterisks show the presence of cristobalite dense phase appeared as a minor phase. ....	110

Figure 5.5	FESEM images of (a) SH4 (w = 2.5), (b) SH7 (w = 3.0) and (c) SH8 (w = 3.5) where the solid products were prepared with a molar composition of $1\text{Al}_2\text{O}_3:w\text{P}_2\text{O}_5:2.5[\text{bzmIm}]_2\text{O}:180\text{H}_2\text{O}:0.47\text{SiO}_2$ heated at 150 °C for 10 h.....	111
Figure 5.6	Particle size distributions of (a) SH4 (w = 2.5), (b) SH7 (w = 3.0) and (c) SH8 (w = 3.5) where the solid products were prepared with a molar composition of $1\text{Al}_2\text{O}_3:w\text{P}_2\text{O}_5:2.5[\text{bzmIm}]_2\text{O}:180\text{H}_2\text{O}:0.47\text{SiO}_2$ heated at 150 °C for 10 h.....	111
Figure 5.7	XRD patterns of (a) SH9 (x = 1.5), (b) SH10 (x = 2.0), (c) SH4 (x = 2.5) and (d) SH11 (x = 3.0) where the solid products were prepared with a molar composition of $1\text{Al}_2\text{O}_3:x\text{P}_2\text{O}_5:x[\text{bzmIm}]_2\text{O}:180\text{H}_2\text{O}:0.47\text{SiO}_2$ at 150 °C for 10 h.....	112
Figure 5.8	FESEM images of (a) SH9 (x = 1.5), (b) SH10 (x = 2.0), (c) SH4 (x = 2.5) and (d) SH11 (x = 3.0) where the solid products were prepared with a molar composition of $1\text{Al}_2\text{O}_3:x\text{P}_2\text{O}_5:x[\text{bzmIm}]_2\text{O}:180\text{H}_2\text{O}:0.47\text{SiO}_2$ at 150 °C for 10 h.....	113
Figure 5.9	Particle size distributions of (a) SH9 (x = 1.5), (b) SH10 (x = 2.0), (c) SH4 (x = 2.5) and (d) SH11 (x = 3.0) where the solid products were prepared with a molar composition of $1\text{Al}_2\text{O}_3:x\text{P}_2\text{O}_5:x[\text{bzmIm}]_2\text{O}:180\text{H}_2\text{O}:0.47\text{SiO}_2$ at 150 °C for 10 h.....	114
Figure 5.10	XRD patterns of (a) SH12 (y = 135), (b) SH4 (y = 180), (c) SH13 (y = 225) and (d) SH14 (y = 270) solid products which were prepared with a molar hydrogel composition of $1\text{Al}_2\text{O}_3:2.5\text{P}_2\text{O}_5:2.5[\text{bzmIm}]_2\text{O}:y\text{H}_2\text{O}:0.47\text{SiO}_2$ at 150 °C for 10 h. ....	116
Figure 5.11	FESEM images of (a) SH12 (y = 135), (b) SH4 (y = 180), (c) SH13 (y = 225) and (d) SH14 (y = 270) solid products which were prepared with a molar hydrogel composition of $1\text{Al}_2\text{O}_3:2.5\text{P}_2\text{O}_5:2.5[\text{bzmIm}]_2\text{O}:y\text{H}_2\text{O}:0.47\text{SiO}_2$ at 150 °C for 10 h. * Tridymite dense phase. ....	116
Figure 5.12	Particle size distribution plots of (a) SH12 (y = 135), (b) SH4 (y = 180), (c) SH13 (y = 225) and (d) SH14 (y = 270) solid products which were prepared with a molar hydrogel composition of $1\text{Al}_2\text{O}_3:2.5\text{P}_2\text{O}_5:2.5[\text{bzmIm}]_2\text{O}:y\text{H}_2\text{O}:0.47\text{SiO}_2$ at 150 °C for 10 h.....	117

Figure 5.13	XRD patterns of (a) SH15 ( $z = 0.0$ ), (b) SH16 ( $z = 0.23$ ), (c) SH4 ( $z = 0.47$ ) and (d) SH17 ( $y = 0.70$ ) prepared with a molar composition of $1\text{Al}_2\text{O}_3:2.5\text{P}_2\text{O}_5:2.5[\text{bzmIm}]_2\text{O}:180\text{H}_2\text{O}:z\text{SiO}_2$ at $150\text{ }^\circ\text{C}$ for 10 h. ....	119
Figure 5.14	FESEM images of (a) SH15 ( $z = 0$ ), (b) SH16 ( $z = 0.23$ ), (c) SH4 ( $z = 0.47$ ) and (d) SH17 ( $y = 0.70$ ) prepared with a molar composition of $1\text{Al}_2\text{O}_3:2.5\text{P}_2\text{O}_5:2.5[\text{bzmIm}]_2\text{O}:180\text{H}_2\text{O}:z\text{SiO}_2$ at $150\text{ }^\circ\text{C}$ for 10 h. ....	120
Figure 5.15	Particle size distributions of (a) SH15 ( $z = 0$ ), (b) SH16 ( $z = 0.23$ ), (c) SH4 ( $z = 0.47$ ) and (d) SH17 ( $y = 0.70$ ) prepared with a molar composition of $1\text{Al}_2\text{O}_3:2.5\text{P}_2\text{O}_5:2.5[\text{bzmIm}]_2\text{O}:180\text{H}_2\text{O}:z\text{SiO}_2$ at $150\text{ }^\circ\text{C}$ for 10 h. ....	121
Figure 5.16	XRD patterns of (a) SH18, (b) SH19, (c) SH4 and (d) SH20 prepared with a molar composition of $1\text{Al}_2\text{O}_3:2.5\text{P}_2\text{O}_5:2.5[\text{bzmIm}]_2\text{O}:180\text{H}_2\text{O}:0.47\text{SiO}_2$ . The samples were heated at 100, 120, 150 and $200\text{ }^\circ\text{C}$ for 10 h, respectively. ....	122
Figure 5.17	SEM images of (a) SH18, (b) SH19, (c) SH4 and (d) SH20 prepared with a molar composition of $1\text{Al}_2\text{O}_3:2.5\text{P}_2\text{O}_5:2.5[\text{bzmIm}]_2\text{O}:180\text{H}_2\text{O}:0.47\text{SiO}_2$ . The samples were heated at 100, 120, 150 and $200\text{ }^\circ\text{C}$ for 10 h, respectively. ....	123
Figure 5.18	Particle size distributions of (a) SH18, (b) SH19, (c) SH4 and (d) SH20 prepared with a molar composition of $1\text{Al}_2\text{O}_3:2.5\text{P}_2\text{O}_5:2.5[\text{bzmIm}]_2\text{O}:180\text{H}_2\text{O}:0.47\text{SiO}_2$ . The samples were heated at 100, 120, 150, and $200\text{ }^\circ\text{C}$ for 10 h, respectively. ....	124
Figure 5.19	Solid yield in percentage with respect to crystallization time. The sample was prepared with a molar composition of $1\text{Al}_2\text{O}_3:2.5\text{P}_2\text{O}_5:2.5[\text{bzmIm}]_2\text{O}:180\text{H}_2\text{O}:0.47\text{SiO}_2$ and heated at $150\text{ }^\circ\text{C}$ (0-14 h). ....	125
Figure 5.20	The hydrothermal crystallization pathway of SAPO-5 templating using $[\text{bzmIm}]\text{OH}$ . ....	128
Figure 6.1	XRD patterns of (a) pristine SAPO-5, (b) $\text{CuCl}_x/\text{SAPO-5}$ , (c) $\text{CoCl}_x/\text{SAPO-5}$ , (d) $\text{SnCl}_x/\text{SAPO-5}$ , (e) $\text{FeCl}_x/\text{SAPO-5}$ and (f) $\text{ZnCl}_x/\text{SAPO-5}$ . ....	133
Figure 6.2	FTIR spectra of (a) SAPO-5, (b) $\text{CuSAPO-5}$ , (c) $\text{CoSAPO-5}$ , (d) $\text{SnSAPO-5}$ , (e) $\text{FeSAPO-5}$ and (f) $\text{ZnSAPO-5}$ . ....	134

Figure 6.3	SEM images and crystal size distributions based on the length of the hexagonal prisms of (a) pristine SAPO-5, (b) CuCl <sub>x</sub> /SAPO-5, (c) CoCl <sub>x</sub> /SAPO-5, (d) SnCl <sub>x</sub> /SAPO-5, (e) FeCl <sub>x</sub> /SAPO-5 and (f) ZnCl <sub>x</sub> /SAPO-5. The selected hexagonal prism crystals in each sample are also highlighted and compared with the theoretical ones. .... 135
Figure 6.4	Possible structures of (a) SAPO-5, (b) CuCl <sub>x</sub> /SAPO-5, (c) CoCl <sub>x</sub> /SAPO-5, (d) SnCl <sub>x</sub> /SAPO-5, (e) FeCl <sub>x</sub> /SAPO-5 and (f) ZnCl <sub>x</sub> /SAPO-5 where the Brönsted acid, Lewis acid and defect sites are denoted as BA, LA and DS, respectively. The arrow and dot line represent the dative and hydrogen bondings, respectively..... 139
Figure 6.5	FriedelCraft acylation of 2-methylfuran and acetic anhydride ..... 144
Figure 6.6	Acylation of 2-methylfuran catalyzed by (a) SAPO-5, (b) CuCl <sub>x</sub> /SAPO-5, (c) CoCl <sub>x</sub> /SAPO-5, (d) SnCl <sub>x</sub> /SAPO-5, (e) FeCl <sub>x</sub> /SAPO-5 and (f) ZnCl <sub>x</sub> /SAPO-5 at 110 °C. Reaction conditions: Catalyst = 0.20 g, 2-methylfuran = 4.7 mmol, acetic anhydride = 14.1 mmol, solvent-free, (Number of experiments = 2). The reaction without adding any catalyst is shown in (g)..... 145
Figure 6.7	Acylation of 2-methylfuran catalyzed by pristine SAPO-5 at (a) 150 °C (b) 160 °C, and (c) 170 °C Reaction conditions: Catalyst = 0.20 g, 2-methylfuran = 4.7 mmol, acetic anhydride = 14.1 mmol, solvent-free, (Number of experiments = 2) ..... 146
Figure 6.8	The Arrhenius linear plots and activation energies (E <sub>a</sub> ) of acylation of 2-methylfuran catalyzed by (a) pristine SAPO-5, (b) CuCl <sub>x</sub> /SAPO-5, (c) CoCl <sub>x</sub> /SAPO-5, (d) SnCl <sub>x</sub> /SAPO-5, (e) FeCl <sub>x</sub> /SAPO-5 and (f) ZnCl <sub>x</sub> /SAPO-5. Reaction conditions: Catalyst = 0.20 g, 2-methylfuran = 4.7 mmol, acetic anhydride = 14.1 mmol, reaction temperature: 90, 100 and 110 °C, time = 0–20 min, solvent-free, (Number of experiments = 2) ..... 147
Figure 6.9	Effect of catalyst loading on acylation of 2-methylfuran catalyzed by ZnCl <sub>x</sub> /SAPO-5. Reaction conditions: 2-methylfuran = 4.7 mmol, acetic anhydride = 14.1 mmol, reaction temperature: 110 °C, time = 20 min, solvent-free. (number of experiments = 2). .... 148

Figure 6.10	Catalytic comparison study between $MCl_x/SAPO-5$ and some common homogeneous catalysts in acylation of 2-methylfuran. Reaction conditions: Catalyst = 0.20 g or equivalent to 110 $\mu$ mol homogeneous catalyst, 2-methylfuran = 4.7 mmol, acetic anhydride = 14.1 mmol, solvent-free, reaction temperature = 110 $^{\circ}C$ , time = 20 min (number of experiments = 2) ..... 151
Figure 6.11	Reusability test of (a) SAPO-5, (b) $CuCl_x/SAPO-5$ , (c) $CoCl_x/SAPO-5$ , (d) $SnCl_x/SAPO-5$ , (e) $FeCl_x/SAPO-5$ and (f) $ZnCl_x/SAPO-5$ for consecutive five reaction cycles. Reaction conditions: temperature = 110 $^{\circ}C$ , time = 20 min, 2-methylfuran = 4.7 mmol, acetic anhydride = 14.1 mmol, catalyst = 0.20 g $MCl_x/SAPO-5.FeCl_3$ ..... 153



## LIST OF SCHEMES

	<b>Page</b>
Scheme 2.1	<i>AlCl</i> <sub>3</sub> activated mechanism of Friede-Crafts acylation reaction [195]..... 46
Scheme 2.2	Acylation of furan derivatives ..... 48

## LIST OF SYMBOL AND NOMENCLATURE

[edmim]OH	1-ethyl-2,3-dimethyl imidazolium hydroxide
(H[Al]Beta)	Lewis acid Beta zeolites
(H[Al]Beta)	Brönsted acid Beta zeolite
AET	Aluminophosphate eight
AFI	Aluminophosphate five
AFO	Aluminophosphate forty-one
Al	Aluminum
AlPO	Aluminophosphate
Al(OiPr) <sub>3</sub>	Aluminum isopropoxide
BEA	Zeolite beta
BET	Brunauer-Emmet-Teller
[bzmIm]Cl	1-benzyl-2,3-dimethyl-1H-imidazole-3-ium chloride
ca.	Circa (approximately)
CHA	Chabazite
CHA	Cyclohexylamine
DFT	Density Functional Theory
DGC	Dry gel conversion
[dhmIm]OTs	3-(2,3-dihydroxypropyl)-1,2-dimethylimidazolium-4-methylbenzene sulfonate
DTG	Derivative thermogravimetry
FAU	Faujasite
Fe	Iron
FESEM	Field emission scanning electron microscopy
FTIR	Fourier transform infrared spectroscopy
GC	Gas chromatography
GHSV	Gas hourly space velocity

HRTEM	High resolution transmission electron microscopy
IUPAC	International Union of Pure and Applied Chemistry
IZA	International Zeolite Association
KCl	Calcium chloride
L/B	Lewis/Brönsted acid ratios
MeAPO	Metalloaluminophosphate
MeAPSO	Metallosilicoaluminophosphate
M	Molarity
MCl <sub>x</sub>	Metal chloride
MeSpa <sup>+</sup> OH <sup>-</sup>	N(16)-methylsparteiniumhydroxide
MS	Mass spectrometry
MTO	Methanol to olefin
<i>n</i>	Framework type
Na <sub>2</sub> CO <sub>3</sub>	Sodium trioxocarbonate
NaCl	Sodium chloride
NaOH	Sodium hydroxide
NMR	Nuclear magnetic resonance
PBU	Primary building unit
[pmIm]Br	1-propyl-2,3-dimethyl-1H-imidazole-3-ium bromide
P	Phosphorous
PP	Polypropylene
RT	Retention time
SAC	Steam assisted conversion
SAPO	Silicoaluminophosphate
SBU	Secondary building unit
SDAs	Structure-directing agents
S <sub>E,int</sub>	Intermediate electronegativity

Si	Silicon
SM1	Substitution mechanism one
SM2	Substitution mechanism two
SM3	Substitution mechanism three
SV	Space velocity
TEA	Triethylamine
TEAOH	Tetraethylammonium hydroxide
TGA	Thermogravimetry analysis xv
TMG	Tetramethylguanidine
TOS	Time on stream
TEM	Transmission electron microscopy
TPA	Tripropylamine
TPD	Temperature programmed desorption
VPT	Vapor phase transport
V <sub>total</sub>	Total pore volume
WHSV	Weight hour space velocity
wt%	Weight percentage
XRD	X-ray diffraction
ZSM-5	Zeolite socony mobile-5

## LIST OF APPENDICES

- APPENDIX A A typical example of calculation of the required masses(g) of the starting materials used in synthesis of SAPO-5 samples
- APPENDIX B Summary of the amounts (g) of chemicals used in preparation of SAPO-5 samples
- APPENDIX C GC-FID chromatograph before reaction (at 0 h)
- APPENDIX D GC-FID chromatograph after reaction in non-microwave instant heating in the presence of ZnCl<sub>2</sub>/SAPO-5 catalyst at (110°C 20 min)
- APPENDIX E GC-MS spectrum of the product, 2-acetyl-5-methylfuran

**ZEOLIT SILIKOALUMINOFOSFAT NOMBOR 5 (SAPO-5) YANG  
DITEMPLATKAN OLEH SEBATIAN IMIDAZOLIUM SEBAGAI  
MANGKIN FRIEDEL-CRAFTS PENGASILAN 2-METILFURAN**

**ABSTRAK**

Silikoaluminofosfat nombor 5 (SAPO-5) adalah salah satu pepejal mikroliang yang dikaji secara meluas kerana penggunaannya sebagai mangkin asid pepejal komersial. Walau bagaimanapun, keasidannya yang sederhana membatasi aktiviti pemangkinnya dalam banyak tindak balas organik yang penting di industri. Objektif penyelidikan ini adalah untuk mensintesis mangkin SAPO-5 menggunakan agen pengarah struktur (SDA) baharu untuk menghasilkan bahan api bio yang berasaskan furan melalui Friedel-Crafts pengasilan 2-metilfuran dengan asetik anhidrida. Kajian ini dimulakan dengan sintesis tiga jenis sebatian imidazolium yang mempunyai kumpulan berfungsi yang berbeza, iaitu 1-propil-2,3-dimetil-1H-imidazol-3-ium ([pmIm]<sup>+</sup>), 1-benzil-2,3-dimetil-1H-imidazol-3-ium ([bzmIm]<sup>+</sup>) dan 3-(2,3-dihidroksilpropil)-1,2-dimetilimidazolium ([dhmIm]<sup>+</sup>) sebelum digunakan sebagai SDA untuk menghablur SAPO-5. Analisis mikroskopi dan spektroskopi menunjukkan bahawa kekutuban dan geometri molekul SDA imidazolium memberi kesan yang ketara dalam sifat fizikokimia produk SAPO-5 yang dihasilkan (contohnya keliangan, luas permukaan, saiz hablur dan morfologi) sementara kadar penghabluran SAPO-5 juga dipercepatkan apabila SDA [dhmIm]<sup>+</sup> yang lebih hidrofilik/berkutub digunakan. Seterusnya, kesan setiap parameter sintesis (suhu, masa pemanasan, nisbah molar P<sub>2</sub>O<sub>5</sub>, SDA [bzmIm]<sub>2</sub>O, SiO<sub>2</sub> dan H<sub>2</sub>O) pada proses penghabluran juga dikaji. Hasil kajian menunjukkan bahawa parameter sintesis mempunyai pengaruh tersendiri terhadap kadar penghabluran, ketulenan hablur, saiz hablur dan morfologi.

Penyelidikan ini juga melaporkan peningkatan keasidan permukaan SAPO-5 melalui percantuman dengan klorida logam ( $\text{CuCl}_2$ ,  $\text{CoCl}_2$ ,  $\text{SnCl}_2$ ,  $\text{FeCl}_3$  dan  $\text{ZnCl}_2$ ) menggunakan kaedah pengisitepuan yang mudah. Analisis menunjukkan bahawa rawatan termokimia selepas pengisitepuan adalah sangat penting untuk pembentukan ikatan kimia yang kuat antara klorida logam dengan SAPO-5. Antara sampel yang telah disediakan,  $\text{ZnCl}_x/\text{SAPO-5}$  dengan tapak asid Lewis yang tertinggi ( $472.6 \mu\text{mol/g}$ , nisbah L/B = 16.1) menunjukkan aktiviti pemangkinan terbaik dalam Friedel-Crafts pengasilan 2-metilfuran (penukaran 94.5%, 100% terpilih kepada 2-asetil-5-metilfuran). Selain itu,  $\text{SnCl}_x/\text{SAPO-5}$ ,  $\text{FeCl}_x/\text{SAPO-5}$  dan  $\text{ZnCl}_x/\text{SAPO-5}$  adalah lebih reaktif daripada mangkin asid homogen biasa ( $\text{H}_2\text{SO}_4$ ,  $\text{HNO}_3$ ,  $\text{CH}_3\text{COOH}$ ,  $\text{FeCl}_3$ ,  $\text{ZnCl}_2$ ) dengan penukaran produk dan penggunaan semula mangkin yang lebih tinggi, seterusnya menawarkannya sebagai proses baharu yang mesra alam dengan pemisahan mangkin yang mudah.

**SILICOALUMINOPHOSPHATES NUMBER 5 (SAPO-5) ZEOLITE  
TEMPLATED BY IMIDAZOLIUM COMPOUNDS AS CATALYST FOR  
FRIEDEL-CRAFTS ACYLATION OF 2-METHYLFURAN**

**ABSTRACT**

Silicoaluminophosphate number 5 (SAPO-5) is one of the most extensively studied microporous solid due its application as commercial solid acid catalyst. However, its weak-to-mild acidity limits its catalytic activity in many industrially important organic reactions. The objective of this research is to synthesize SAPO-5 catalyst using new imidazolium-based structure-directing agents (SDAs) for producing furan-based biofuel *via* Friedel-Crafts acylation of 2-methylfuran with acetic anhydride. The study began with the synthesis of three types of imidazolium compounds bearing different functional groups, *viz.* 1-propyl-2,3-dimethyl-1H-imidazole-3-ium ([pmIm]<sup>+</sup>), 1-benzyl-2,3-dimethyl-1H-imidazole-3-ium ([bzmIm]<sup>+</sup>) and 3-(2,3-dihydroxypropyl)-1,2-dimethylimidazolium ([dhmIm]<sup>+</sup>) to be used as SDAs to crystallize SAPO-5. The microscopic and spectroscopic analyses showed that the polarity and molecular geometry of imidazolium SDAs significantly governed the physicochemical properties of the resulting SAPO-5 products (e.g. porosity, surface area, particle size, and morphology). Among the SDAs, the [dhmIm]<sup>+</sup>, which has the highest hydrophilicity/polarity, demonstrated fastest crystallization rate of SAPO-5 due to its diol group that withdraw electron density from imidazolium ring, thereby increasing the templating effect. Next, the effects of each synthesis parameters (temperature, heating time, molar ratios of P<sub>2</sub>O<sub>5</sub>, [bzmIm]<sub>2</sub>O SDA, SiO<sub>2</sub>, and H<sub>2</sub>O) on the crystallization process is also investigated. The results indicate that the synthesis parameters influence the crystallization rate, purity, crystal size and morphology. The



research also reports on the enhancement of surface acidity of SAPO-5 by grafting with metal chlorides ( $\text{CuCl}_2$ ,  $\text{CoCl}_2$ ,  $\text{SnCl}_2$ ,  $\text{FeCl}_3$ , and  $\text{ZnCl}_2$ ). The analysis shows that the thermochemical treatment after impregnation is essential for the formation of strong chemical bonding between the metal chlorides and SAPO-5. Among samples prepared,  $\text{ZnCl}_x/\text{SAPO-5}$  with the highest Lewis acid site amount (472.6  $\mu\text{mol/g}$ , L/B ratio = 16.1) shows the best catalytic activity in the Friedel-Crafts acylation of 2-methylfuran (94.5% conversion, 100% selective to 2-acetyl-5-methylfuran) under non-microwave instant heating condition. In addition,  $\text{SnCl}_x/\text{SAPO-5}$ ,  $\text{FeCl}_x/\text{SAPO-5}$  and  $\text{ZnCl}_x/\text{SAPO-5}$  are more reactive than the common homogeneous acid catalysts ( $\text{H}_2\text{SO}_4$ ,  $\text{HNO}_3$ ,  $\text{CH}_3\text{COOH}$ ,  $\text{FeCl}_3$ ,  $\text{ZnCl}_2$ ) with higher reactant conversion and catalyst reusability up to four cycles, offering new environment-friendly process with a facile catalyst separation.

# CHAPTER 1

## INTRODUCTION

### 1.1 General Introduction

The world's major oil fields are becoming depleted [1]. According to the 2019 Geological Survey of Finland report, the global oil production could drop to half its current volume around 2030-2034 [2]. Thus, the continuous dependence on fossil carbon energy sources will result in a tremendous energy crisis in the near future [1].

Biofuel derived from biomass sources (cellulose and hemicellulose) is an excellent renewable resource having zero CO<sub>2</sub> emission [3]. Recently, there has been an increasing demand for biofuel globally [4]. Biofuel is produced through the conversion of biomass to fuel using thermal, thermochemical, or biothermal processes [5]. Nevertheless, the downsides of these processes are high energy-consumption and expensive.

Catalytic conversion reaction is another promising alternative to produce biofuel [6]. In particular, furan-based fuel is regarded as a second-generation biofuel owing to its high-octane number and high energy density [5, 7]. Typically, furan-based biofuel can be obtained through catalytic conversion involving Friedel-Crafts acylation [8, 9].

Classically, Friedel-Crafts acylation reaction is catalyzed using homogeneous Lewis acids such as AlCl<sub>3</sub>, FeCl<sub>3</sub>, and TiCl<sub>4</sub> [10, 11], and Brønsted acid such as HF, H<sub>2</sub>SO<sub>4</sub>, H<sub>3</sub>PO<sub>4</sub> [12, 13]. Unfortunately, these homogeneous acids suffer from several drawbacks, including safety issues (high toxicity and corrosive), environmental pollution (large waste production and energy consumption), product separation

difficulty, and low catalyst reusability [14-16].

Silicoaluminophosphates (SAPO- $n$ , where  $n$  is the framework type) are crystalline microporous solids which were first discovered by Lok and co-workers from Union Carbide Corporation in 1984 [17]. SAPO- $n$  play a major role in the ion-exchange, separation and catalytic processes owing to their Brønsted acidity and shape-selectivity [18-20]. In addition, their flexible synthesis conditions and techniques allow systematic control of their physicochemical properties (crystallinity, porosity and morphology) that directly affect their catalytic behavior [21].

Among SAPO- $n$  materials, silicoaluminophosphate number 5 (SAPO-5) is the most useful zeotype material due to its large micropores. Typically, SAPO-5 can be hydrothermally synthesized in the presence of triethylamine, tripropylamine, tetraethylammonium hydroxide, tetrabutylammonium hydroxide or *N*-methyldicyclohexylamine as structure-directing agents (SDA) [22-26]. The crystallization usually occurs at 180-200 °C and requires long heating time (in days) which is considerably time and energy-consuming [27-30].

Recently, imidazolium-based SDAs have been used as both SDA and solvent in the ionothermal crystallization of SAPO-5 [31], SAPO-34 [32], and SAPO-11 [31]. Imidazolium cations are valuable templates due to their strong host-guest interactions [33]. The nature of the organic functional group attached to the imidazolium ring and the geometry have been found to influence the formation of novel zeolite structures under certain reaction conditions [32]. Recently, the study on the utilization of imidazolium cations to develop novel zeolite structures has gained significant attention [34-36]. Nevertheless, the interactions between SDAs and the zeolite/zeotype crystal phase are not yet very clear. But it is known that these organic molecules direct the

formation of the inorganic framework [23]. A systematic investigation of SDA-framework interaction hence can provide insight on controlled synthesis of AlPO-n/SAPO-n materials bearing different morphologies and crystal sizes [24, 32].

Moreover, a detailed work on the study of the influence of synthesis parameters on the formation of SAPO-5 crystals under hydrothermal conditions, particularly using imidazolium-based SDAs is rarely found in the literature [37]. In addition, SAPO-5 is preferable as a solid catalyst for catalyzing acylation of furan because it tends to give higher product selectivity as compared to conventional zeolites. The factors responsible for SAPO-5 selectivity are mild acid strength which provides adsorption of molecules onto catalyst active sites with moderate strength. This enhances the stability of the active site and prolongs the catalyst lifespan. Secondly, the tubular pore system of SAPO-5 gives rise to inverse shape selectivity where larger molecules can easily diffuse into the pore and access to the active sites [38]. However, its mild acid strength always gives low reaction conversion. Hence, surface modification is needed to enhance the surface acid strength of SAPO-5.

Several techniques have been identified as promising approaches to enhance the surface acid strength such as functionalization of organic acids [39], isomorphous substitution of heteroatoms [40-42], dealumination [43, 44], grafting [45], and post-synthesis treatments [45, 46]. In particular, grafting of metal chlorides on solid supports is an effective approach to enhance the surface acidity of the solid catalysts [47-51]. However, the disadvantage of this technique is the leaching of the metal salts from the solid support during the catalytic reaction due to the weak chemical interaction between the support and the metal salt [52]. Hence, designing a promising solution to this problem would be of great interest. Furthermore, the effects of incorporation of metal chlorides on SAPO-5 and its catalytic performance in Friedel-

Crafts acylation of furan derivative are not known thus far, and hence, comprehensive work on this study is worth being further explored.

Chemical reactions are carried out in various types of reactors using catalysts in order to increase the reaction rate and improve conversion. The reaction rate is temperature-dependent thus it is strongly influenced by heat transfer. The conventional reflux system is the most commonly employed reactor due to its simplicity, safety and ease of separation [53]. However, this method is time-consuming due to its ineffective heat transfer mechanism [54]. On the other hand, non-microwave instant heating is a modern heating technique that uses silicon carbide (SiC) as a reaction vessel that can heat the reaction mixture very rapidly where the overall heating rate is nearly equivalent to that of a microwave system [55]. SiC is used because it is an excellent thermal conductive and effusive material that can rapidly exchange thermal energy with the surrounding. Thus, the heat transfer from the reactor to the reaction vessel is extremely fast, and the heating process is accelerated.

## **1.2 Research objectives**

The objectives of this research are:

- (a) To synthesize three novel imidazolium SDAs with propyl, benzyl and diol functional groups. The compounds are then used as organic templates to synthesize SAPO-5 crystals.
- (b) To study the influence of the propyl, benzyl and diol functional groups of SDAs on the physicochemical properties and crystallization profiles of SAPO-5.

- (c) To Investigate the effects of synthesis parameters (e.g. initial gel composition, heating temperature and time) on the crystallization processes of SAPO-5 crystals.
- (d) To enhance the acidity of SAPO-5 *via* grafting of various metal chlorides.
- (e) To investigate the catalytic behavior of pristine and metal chlorides grafted SAPO-5 solid catalysts in Friedel-Crafts acylation of 2-methylfuran with acetic anhydride under non-microwave instant heating condition.

### **1.3 Thesis overview**

This thesis is composed of seven chapters, in which a brief description of the project background, literature survey, experimental procedure and research findings are discussed. Chapter One provides the general outlook of the research, where basic introduction of biofuel, porous materials, zeolites and zeolite-like materials are introduced. The chapter also covers problem statements and the objectives of study.

Chapter Two contains a comprehensive literature survey with a focus on the research topic. This chapter covers more detailed aspects of zeolite chemistry and narrowed to the literature review of the reported studies on SAPO-*n* microporous solids, including synthesis methods, effects of synthesis parameters on SAPO-*n* crystallization, importance and effects of structure-directing agents, as well as applications of SAPO-5 solids in various fields. Lastly, the literature study about Friedel-Crafts acylation reaction is also presented.

The experimental methodology employed to carry out the entire project is

compiled in Chapter Three. This includes the synthesis procedure for three types of imidazolium-based templates, namely 1-propyl-2,3-dimethyl-1H-imidazole-3-ium bromide ([pmIm]Br), 1-benzyl-2,3-dimethyl-1H-imidazole-3-ium chloride ([bzmIm]Cl) and 3-(2,3-dihydroxypropyl)-1,2-dimethylimidazolium-4-methylbenzene sulfonate ([dhmIm]OTs) which are subsequently converted into [pmIm]OH, [bzmIm]OH and [dhmIm]OH as SDA solutions *via* ion exchange treatment. Furthermore, the synthesis protocol of SAPO-5 is also described in this chapter. Besides, the experimental procedures of the synthesis parameter study and metal chlorides grafting experiment are also described. Lastly, the details of the characterization techniques used, including their principle of operation and the analysis conditions are also provided.

Chapter Four discusses the results of the synthesis of SAPO-5 using [pmIm]OH, [bzmIm]OH, and [dhmIm]OH SDAs where the effects of their functional groups on crystallization profiles and morphology of SAPO-5 are carefully investigated. In addition, the discussion on the influence of these templates on porosity and chemical composition of the synthesized SAPO-5 is also reported.

Chapter Five deals with the findings of the study of synthesis parameters (crystallization time, heating temperature, and composition of starting reagents) on the crystallization of SAPO-5. The results of the analysis are then used to propose a possible formation mechanism of SAPO-5 microporous material mainly based on spectroscopic and microscopic observations.

Chapter Six discloses the results of the study of metal chlorides grafted SAPO-5 as superior and reusable catalysts in the acylation of 2-methylfuran where acetic anhydride is used as an acylating agent. Five different types of metal chlorides grafted SAPO-5 were used in this study, namely, SnCl<sub>x</sub>/SAPO-5, FeCl<sub>x</sub>/SAPO-5, ZnCl<sub>x</sub>/SAPO-5, CuCl<sub>x</sub>/SAPO-5 and CoCl<sub>x</sub>/SAPO-5 the prepared samples are then characterized using XRD, SEM, EDX, FT-IR, pyridine adsorption and nitrogen adsorption analysis. Furthermore, the influence of the grafted species on the acidity of all the samples is discussed based on the pyridine adsorption results. The catalytic reaction was then performed free of solvent and using a non-microwave instant heating method. In this chapter, the catalytic reaction parameters such as heating time and temperature, catalyst loading, heating methods and so on are also discussed.

Lastly, Chapter Seven highlights the overall findings of the research. Moreover, some recommendations for future research works in this project are also given.



## CHAPTER 2

### LITERATURE REVIEW

#### 2.1 Microporous zeolites

Porous materials are solid materials infused by interlinked or non-interlinked pores where the term pores are referred to cavities, channels or interstices. The International Union for Pure and Applied Chemistry (IUPAC) has classified porous materials into three classes based their pore sizes, namely micropore as materials with pore size  $< 2$  nm (e.g. zeolites, pillared clays), mesopore with pore size 2-50 nm (e.g. MCM-41, SBA-15), and macropore having pore size  $>50$  nm (e.g. ceramic-based materials, porous glasses) (Figure 2.1) [56].

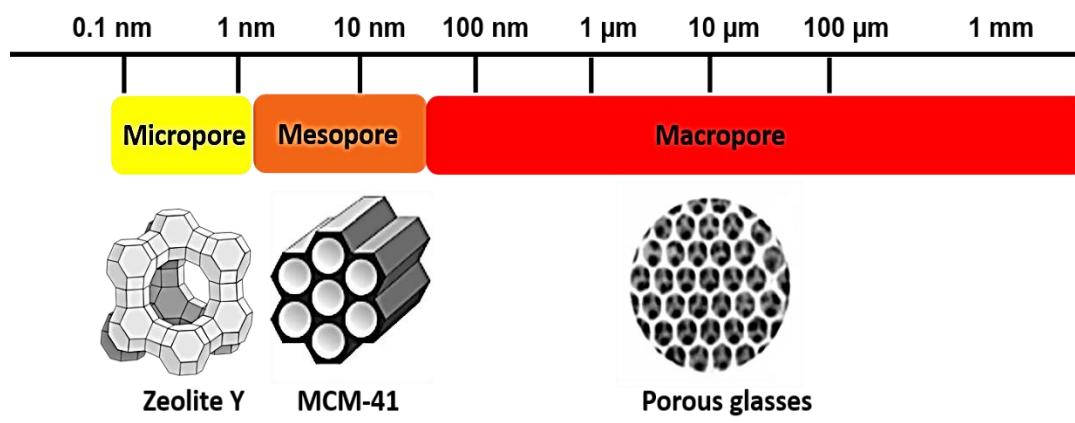


Figure 2.1. Illustration of the IUPAC classification of porous materials [57]

Zeolites are crystalline microporous materials. They can simply be described as a class of hydrated aluminosilicates made up of aluminate  $[\text{AlO}_4]^{5-}$  and silicate  $[\text{SiO}_4]^{4-}$  each existing in tetrahedral geometry with an oxygen atom covalently bonded to the neighboring tetrahedral, and producing a giant three-dimensional (3D) microporous structure (called framework) having cavities of varying shape and sizes

[58] (Figure 2.2). The zeolite's framework is associated with a net negative charge. This charge imbalance is due to the substitution of  $\text{Si}^{4+}$  by  $\text{Al}^{3+}$  as a consequence of the difference in the formal charge of  $[\text{AlO}_4]^{5-}$  and  $[\text{SiO}_4]^{4-}$  species. Hence, a charge compensating cations  $\text{M}^+$  is required to neutralize the negative charge and maintain the electrical neutrality [59]. This generates a Brønsted acid site on the neighboring oxygen atom when  $\text{M}^+$  is a proton ( $\text{H}^+$ ). Moreover, the compensating cation can be exchanged by other metal ions such as  $\text{Na}^+$ ,  $\text{K}^+$ ,  $\text{NH}_4^+$ ,  $\text{Li}^+$  and  $\text{Cs}^+$ .

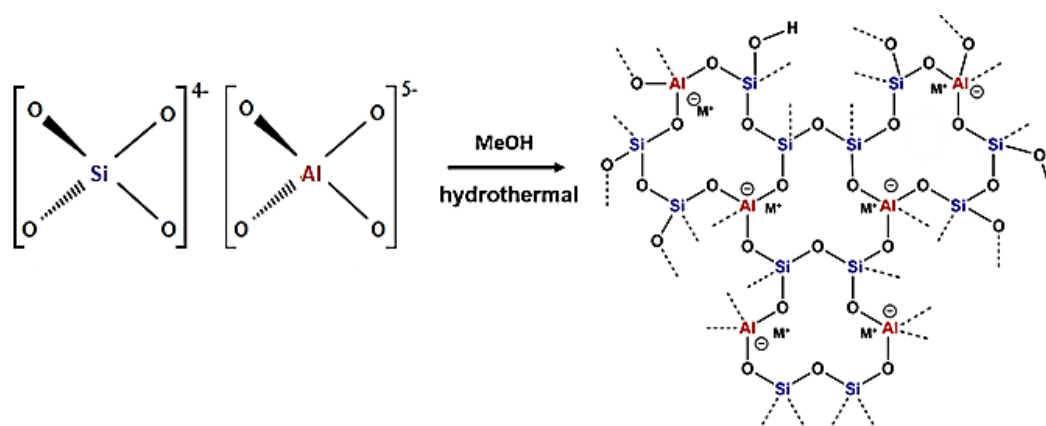
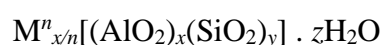


Figure 2.2. The formation for zeolite framework where MeOH is metal hydroxide of group I or II that provide the compensating cation  $\text{M}^+$  [60].

Owing to the unique shape and size of zeolite pores, acidity/basicity, and ion-exchange properties, zeolites have emerged as good candidates as shape-selective catalysts, adsorbents and ion exchangers. This microporous material has thus been commercialized and produced in large scale for industrial use [61, 62]. The general chemical formula of zeolites can be written as



where M is group I or II exchangeable metal cation with  $n$  charge balance, while  $x$ ,  $y$ , and  $z$  are the numbers of moles of  $\text{AlO}_2$ ,  $\text{SiO}_2$  and  $\text{H}_2\text{O}$ , respectively.

In the zeolite structures, the primary building units (PBUs) build up the secondary building units (SBUs), where the systematic connection of different SBUs finally leads to a complete zeolite crystalline structure with a unique framework pore and channels (Figure 2.3). So far, there are more than 250 types of zeolite frameworks discovered and these zeolite frameworks are named systematically according to the protocol set by the Structure Commission of the International Zeolites Association (IZA) according to IUPAC nomenclature.

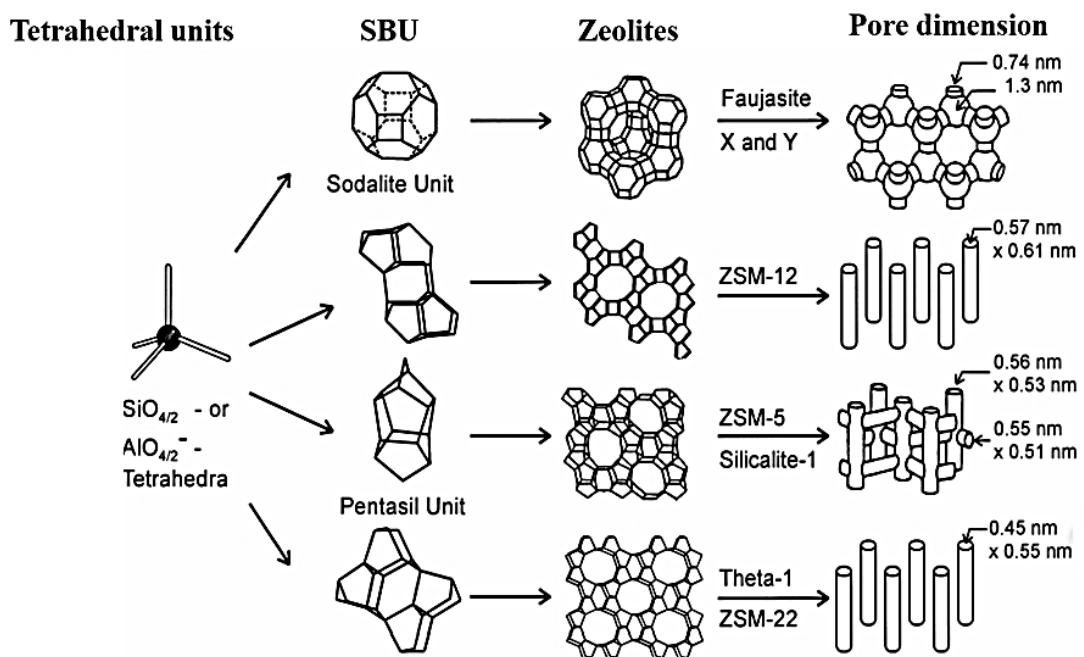


Figure 2.3. Building units of zeolites and the framework structures of zeolites [63]

Thus, each zeolite material is given a three-letter code, which is absolutely unique to a specific framework (topology). For example, zeolite Beta is given framework code **BEA** extracted from its IUPAC name **B**eta polymorph **A**. Other examples are **Faujasite** zeolite: **FAU**, **Mordenite** zeolite: **MOR**, zeolite L: **LTL** (**L**inde type **L**) [64].

### 2.1.1 Formation of zeolite

In nature, zeolites are usually formed from volcanic activity. The volcanoes erupt lava and a huge deposit of ash composing of aluminosilicate is produced. This ash and lava often mix with nearby water bodies (often semi-saline water containing alkaline metal salts). If the chemistry of the water is suitable (pH and composition), the hot lava, ash and saltwater will undergo reaction for thousands or millions of years under high temperature and pressure, and consequently, the zeolite crystalline solids are formed [60]. Natural zeolites have remarkable physicochemical properties and are found in different regions of the world. Presently, there are 67 different types of zeolite minerals discovered thus far, where clinoptilolite is the most abundant natural zeolite with significant commercial value [65, 66].

Zeolites can also be formed under a synthetic route called hydrothermal conditions. So far, the application of hydrothermal synthesis technique has also been extended to the synthesis of zeolite-like materials such as silica mesoporous materials (e.g. MCM-41, MCM-48, HMS, SBA-15), metal-organic frameworks (MOFs), aluminophosphate (AIPO-n), silicoaluminophosphate (SAPO-n) and metalloaluminophosphate (MeAPO-n).

## 2.2 Aluminophosphate (AIPO-*n*) and silicoaluminophosphate (SAPO-*n*) zeotypes

Zeotypes are family of solids possessing identical framework structure to zeolites but having different chemical compositions. In another word, zeotype refers to collective name of microporous zeolites and related compounds, where the silicon atom in the framework is partly or fully replaced by Al and/or P and or metal [67].

Aluminophosphates (AIPO-*n*) are the first zeotype family free of silica. In the early 1980s, AIPO-*n* was first reported by Wilson and co-workers at Union Carbide [68]. Similar to zeolites, each member of the AIPO-*n* material is identified by a unique name set by International Zeolite Association (IZA), where the *n* denotes a specific framework type, and is followed by the three-letter framework code. Examples AIPO-5 = **AFI** (AIPO **F**ive), and AIPO-8 = **AET** (AIPO **E**ight). The analogous SAPO-*n* (discussed in subsequent section) are also named in similar fashion, e.g. SAPO-5 = **AFI** (SAPO **F**ive), SAPO-41 = **AFO** (SAPO **F**orty-**O**ne). However, some AIPO-*n* and SAPO-*n* are exempted in this naming concept, because they have identical framework structure with conventional aluminosilicate zeolites. For instance, AIPO-37 and SAPO-37 have a framework code of **FAU**, named after zeolite **Fau**jasite due to the same framework structure. Example of some selected AIPO-*n* materials with their pore dimensions are given in Table 2.1. Out of over 250 known zeolite frameworks, about 60 can only be prepared in AIPO-*n* or SAPO-*n* form [64].

Similar to the mode of formation of zeolites, the AIPO-*n*/SAPO-*n* materials are built from preformed building blocks termed secondary building units (SBUs) (Table 2.1, Figure 2.4). The SBUs can compose up to 16 tetrahedral atoms (P, Al, and Si) assuming that a framework is built from one type of SBUs [65]. The SBUs are achiral

structures, as indicated in Figure 2.4, the straight lines represent the bonding between two tetrahedral atoms while omitting the oxygen atoms for simplicity [69].

Table 2.1

*Some AlPO-n/SAPO-n based molecular sieves*

<i>n</i>	Framework code	Framework type	Pore dimension (nm) <sup>2</sup>
<b>Extra-large pore</b>			
VPI-5	VFI	Novel	1.27 × 1.27
8	AET	Novel	0.79 × 0.87
<b>Large pore</b>			
5	AFI	Novel	0.73 × 0.73
36	ATS	Novel	0.62 × 0.75
37	FAU	Faujasite	0.74 × 0.74
40	AFR	Novel	0.67 × 0.69
46	AFS	Novel	0.7 × 0.7
<b>Medium pore</b>			
11	AEL	Novel	0.4 × 0.65
31	ATO	Novel	0.54 × 0.54
41	AFO	Novel	0.43 × 0.7
<b>Small pore</b>			
14	AFN	Novel	0.31 × 0.43
17	ERI	Erionite	0.36 × 0.51
18	AEI	Novel	0.38 × 0.38
25	ATV	Novel	0.3 × 0.49
33	ATT	Novel	0.42 × 0.46
34, 44, 47	CHA	Chabazite	0.38 × 0.38
35	LEV	Levynite	0.38 × 0.48
39	ATN	Novel	0.4 × 0.4
<b>Very small pore</b>			
25	ATV	Novel	0.3 × 0.49

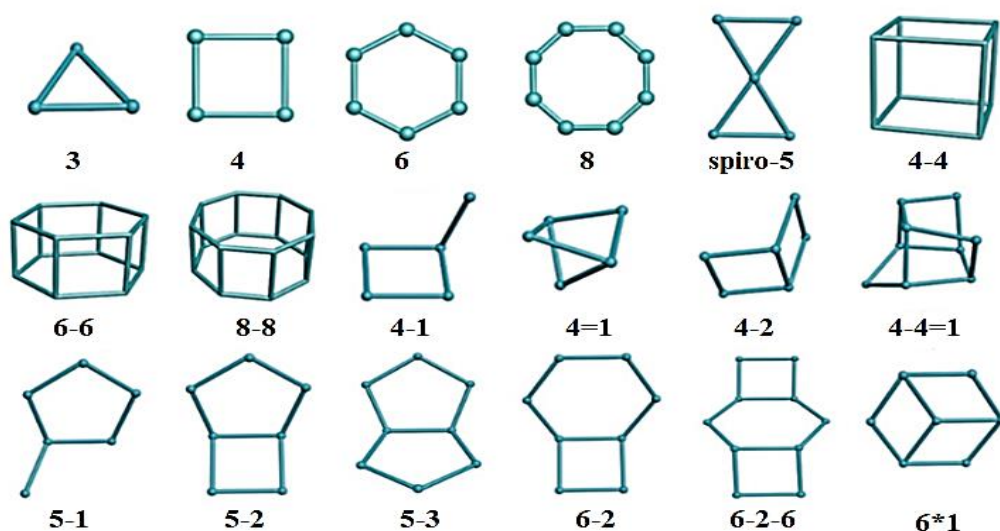


Figure 2.4. The types of secondary building units (SUBs) found in zeolitic frameworks [69]

Although zeolites and AlPO-*n* are similar in many respects, however, their chemistry is quite different. Zeolites are generally synthesized in alkaline conditions (pH ~ 8-14), which is suitable for deprotonation of a silanol group, lower pH may lead to a dense phase of aluminosilicates. On the other hand, AlPO-*n* require less acidic or neutral condition (pH ~ 6-8) for crystallization [70]. The phosphorous source for the synthesis of AlPO-*n* is usually orthophosphoric acid, whereas zeolite uses various silica sources (e.g fumed silica, colloidal silica). Thus, the precursor gel of AlPO-*n* is favored by low pH while that of zeolite tends to be more basic. Nevertheless, the gel chemistry is also influenced by the use of structure directing agent (SDA) (e.g. tetraethylammonium hydroxide (TEAOH), triethylamine (TEA), etc.) [71, 72].

Secondly, the net charge of the zeolite framework is negative, thus requires a compensating cation as explained earlier. On the contrary, the framework of AlPO-*n* is neutral because it is constructed by corner-sharing of tetrahedra of a negatively charged aluminate and a positively charged phosphate. Therefore, to introduce an

acidic character in AlPO-*n* (for use as a catalyst), modification is carried out through isomorphous substitution of metals such as Si, Fe as in SAPO-5, and FeAPO-5, respectively [73].

Furthermore, the framework of zeolites is built by [Si-O-Si] and [Si-O-Al] linkages, while that of AlPO-*n* is constructed by an alternating [Al-O-P] and [P-O-Al] units. No [Al-O-Al] or [P-O-P] repeat units are allowed in the AlPO-*n* framework structures [74, 75] (Figure 2.5). Another difference is that high silica zeolites are hydrophobic materials, whereas AlPO-*n* are mildly hydrophilic due to the electronegativity difference between P (2.19) and Al (1.61).

The interesting property of AlPO-*n* molecular sieve is that the Al and P in the framework can be partly substituted by other heteroatoms such as Si. This process is called isomorphous substitution. When the Si atom is introduced as a heteroatom, silicoaluminophosphate (SAPO-*n*) materials are produced [17] (Figure 2.5). Similarly, metals (such as Zn, Cu, Fe, Pd) can also be isomorphically substituted into both AlPO-*n* and SAPO-*n* to yield metalloaluminophosphate (MeAPO-*n*) and metallosilicoaluminophosphate (MeAPSO-*n*), respectively [72].

AlPO-*n* and SAPO-*n* have identical topology. Thus, for each AlPO-*n* framework, there exists a SAPO-*n* analogous. For example, AlPO-5 and SAPO-5 have same topology (AFI), they can be synthesized using the same SDA, in the same mildly acidic environment. The incorporation of Si atom during crystallization under hydrothermal conditions brings about the acidic property which makes SAPO-*n* family a superior solid catalyst over the corresponding AlPO-*n* [72].



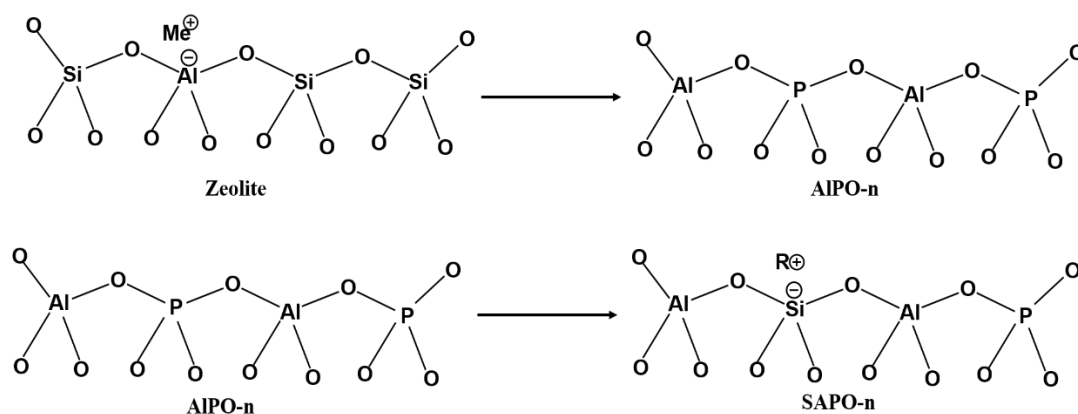
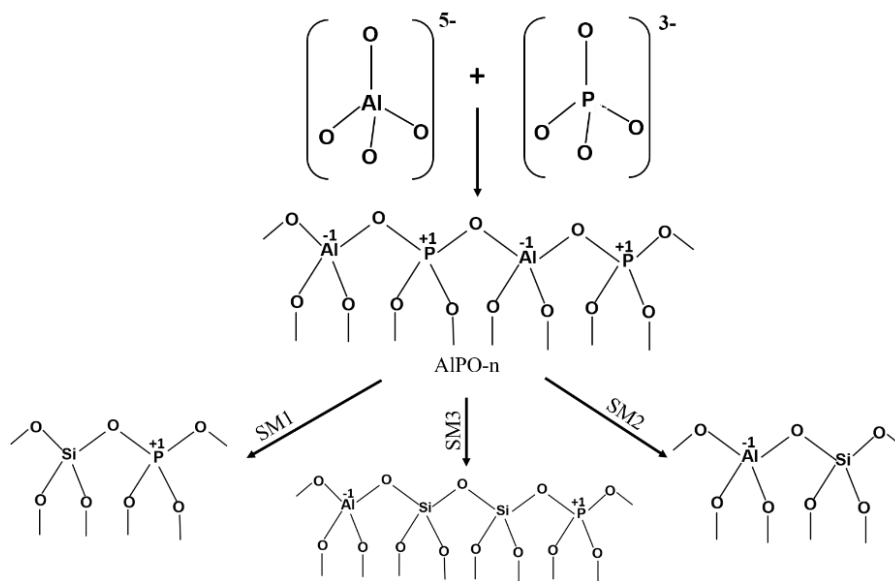


Figure 2.5. Arrangement of tetrahedra in zeolite, AIPO-n, and SAPO-n molecular sieves, where  $\text{Me}^+$  and  $\text{R}^+$  are counter cation and structure directing agent, respectively

### 2.2.1 Mechanism of Si isomorphous insertion

There are three different possibilities of isomorphous substitution mechanisms (SM) of Al and P that take place in AIPO-*n* microporous structure. The first mechanism (SM1) is where Si substitutes Al, the second mechanism (SM2) where Si substitutes P, while the third mechanism (SM3) where two Si simultaneously substitutes P and Al [76-78] (Figure 2.6).

During SM1 process (Si→Al substitution), the  $\text{Al}^{3+}$  is replaced by  $\text{Si}^{4+}$ . This results in the emergence of a positively charged framework, and thus [Si-O-P] linkage is formed (Figure 2.7a). However, the SM1 situation is very unlikely to occur considering the reaction condition and the cationic nature of the organic SDA used. Hence, the process is thermodynamically unfavorable, making the formation of [Si-O-P] linkage not feasible [74].



*Figure 2.6.* General substitution mechanism of Si atom in AlPO-*n* molecular sieves

For SM2 (Si→P substitution), a  $\text{Si}^{4+}$  would replace a  $\text{P}^{5+}$  in tetrahedral coordination, and consequently a framework with an evenly distributed Si is generated. SM2 gives rise to four [Al-O-Si] linkages where one of the oxygen atoms bonded to Si is attached to a proton as a charge balancer (Figure 2.7b). The presence of -OH group bring about the Brönsted acidity of the SAPO material

Furthermore, in SM3 (2Si→P, Al substitution), the P and Al are being replaced by two Si atoms, which results in the generation of so-called silicon island. When this substitution occurs, two Si tetrahedron sites of a different chemical environment are produced. The chemical environment of the newly formed Si tetrahedron depends on the neighbor tetrahedron sites. Therefore, the first Si tetrahedral coordination sphere may either be Si(4P), Si(4Al) (Figure 2.7c), or Si(3Al,1Si), Si(3P,1Si) (Figure 2.7d). Moreover, another possibility of silicon island formation is when two atoms each of P and Al are replaced by four Si. This leads to two types of arrangements; the linear

(Figure 2.7e) and the four tetrahedral ring arrangement (Figure 2.7f).

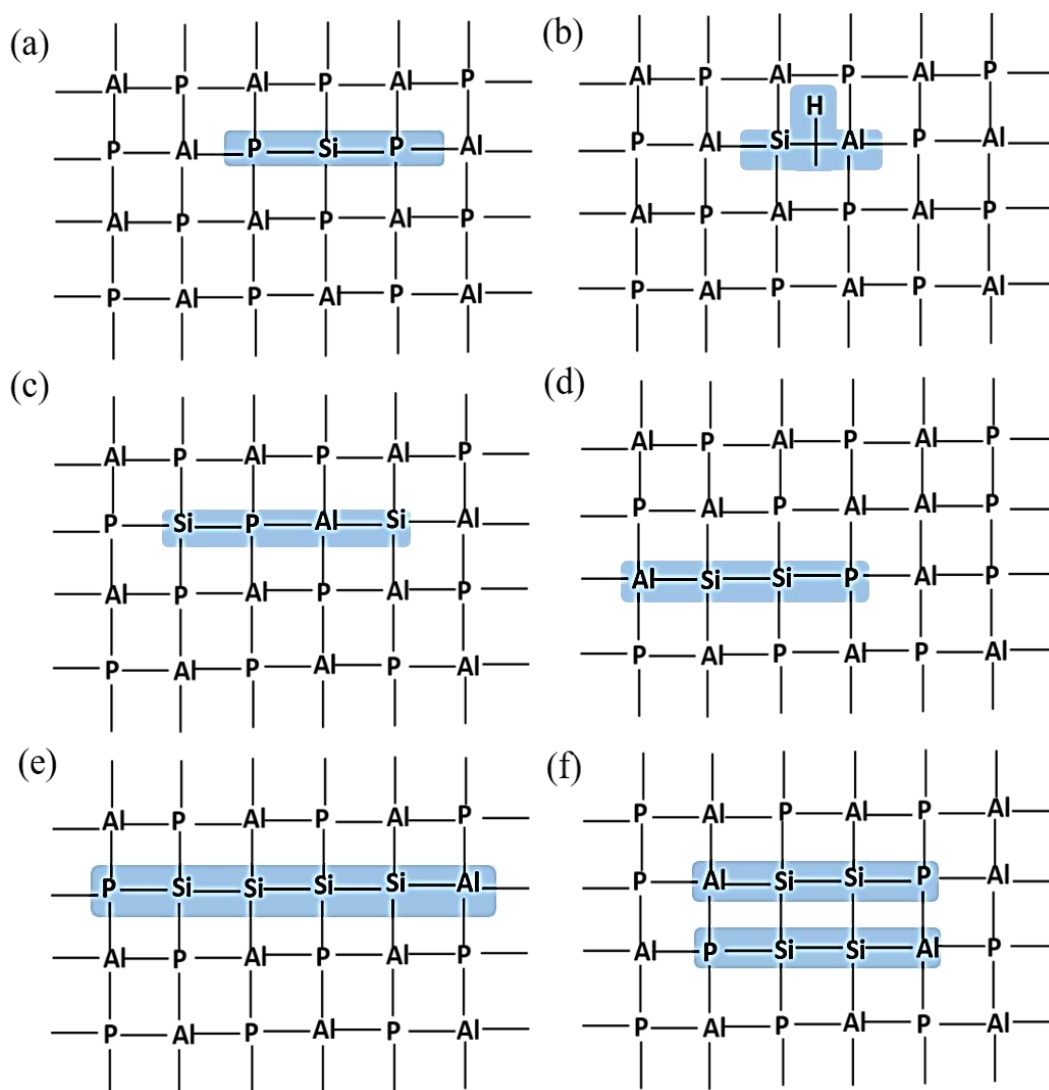


*Figure 2.7.* A 2D representation of various mechanisms of Si insertion in AlPO-*n* framework: **(a)** SM1: Si→Al substitution, **(b)** SM2: Si→P substitution, and **(c)** SM3: 2Si→P,Al substitution which further divides into **(d)** SM3: 2Si→P,Al (generation of island), **(e)** SM3: 4Si→2P,2Al (generation of line), and **(f)** SM3: 4Si→2P,2Al (generation of ring). The oxygen atoms are not shown for simplicity.

### 2.3 SAPO-5 microporous materials

Silicoaluminophosphate number 5 (SAPO-5) is a large pore zeolite consisting of one dimensional 12 membered-ring channel system. This AFI-type molecular sieve has a parallel pore with a dimension of  $0.73 \times 0.73 \text{ nm}^2$ . The framework can be constructed from either of the secondary building units 4, 6 or 12. Alternatively, it can be visualized as comprising any of the SBUs *bog*, *afi* or the *nsc* (narsarsukite) chain (Figure 2.8) [65, 79, 80]. SAPO-5 is one of the most extensively studied SAPO-*n* materials due to its facile crystal formation and less selectivity of SDA, where it can be synthesized using more than 25 different SDAs [81, 82].

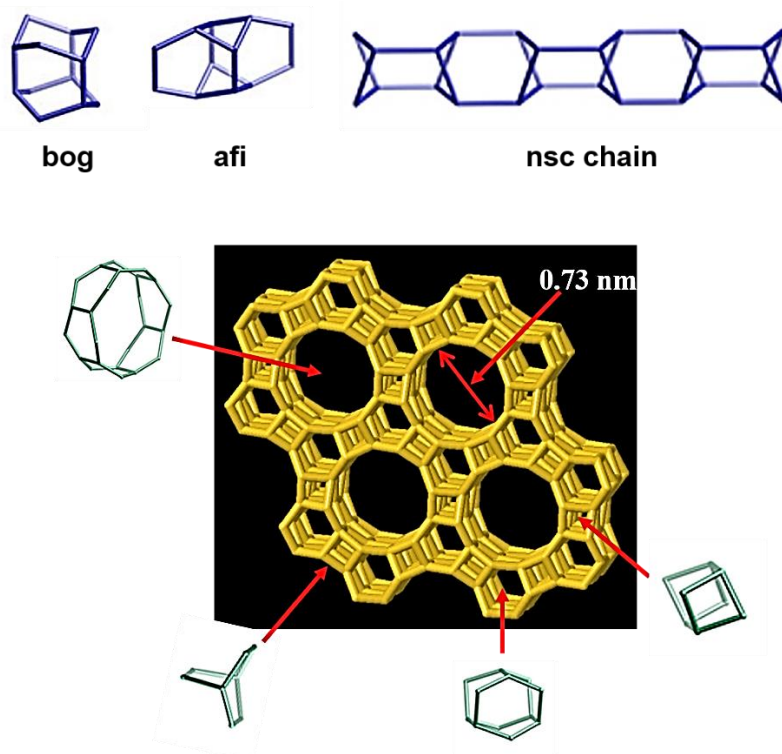


*Figure 2.8.* A typical SAPO-5 framework with AFI topology formed by the assembly of several secondary building units. The CBUs present in the AFI structure are displayed in the top row, with the framework oxygens omitted for clarity. [83]

SAPO-5 material was first synthesized by Lok and co-workers from Union Carbide in 1984 [17]. Since its discovery, several organic amines have been identified as a suitable SDA for crystallization of AFI framework structure. The common examples are tripropylamine, triethylamine, tetraethylammonium hydroxide, and di-n-propyl amine [84-88]. Unlike other AlPO-n/SAPO-n, SAPO-5 has high thermal and hydrothermal stabilities where the crystals can stand a heat treatment of up to ~750 °C in both dry and moist atmospheres [89, 90], hence can withstand harsh reaction conditions.

Morphological properties play a vital role in many catalytic reactions as they provide different diffusion path lengths and affect the catalytic efficiency [91]. The morphology of SAPO-5 crystals are commonly hexagonal shaped [22]. Interestingly, many studies have shown the possibility of tuning this morphology into various shapes by using different SDAs [92-94]. For instance, SAPO-5 of hexagonal prism [95], plate-like [96] and hexagonal rod-like [97, 98] morphologies can be synthesized using triethylamine, tetraethylammonium bromide and tripropylamine organic templates, respectively, under either hydrothermal or microwave heating conditions. Furthermore, the tailoring of the crystal morphology can also be achieved by varying the source and composition of starting materials or altering the pH condition of the synthesis mixture (neutral, basic or acidic) [88, 96]. Figure 2.9 show some typical examples of SAPO-5 crystals exhibiting different morphologies resulted from synthesis using different starting materials or pH.

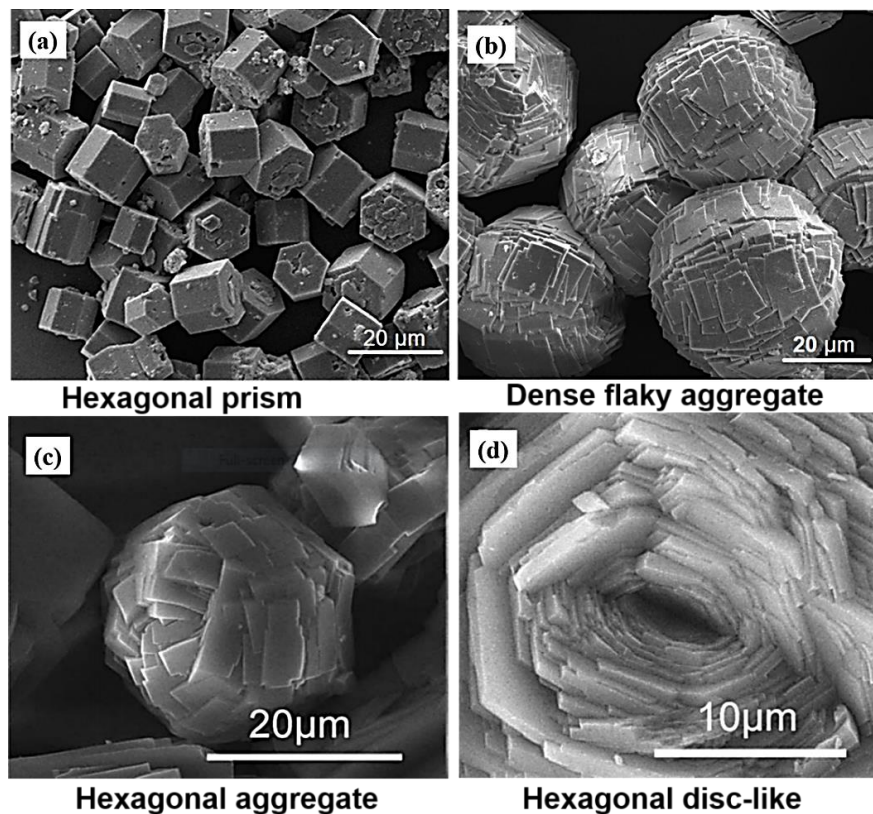


Figure 2.9. SAPO-5 crystals synthesized using different Al sources: (a) aluminum isopropoxide and (b) pseudo boehmite [99], and those synthesized at different pH using aluminum isopropoxide as Al source: (c) pH 9 and (d) pH 7 [22].

### 2.3.1 Synthesis of SAPO-5 molecular sieves

#### 2.3.1(a) Dry-gel conversion method

A dry gel conversion (DGC) is common technique for the crystallization of SAPO-5 and other porous materials [100-103]. The DGC was first reported by Xu *et al.* in 1990 [104]. Typically, the DGC technique involves the preparation of the reaction gel followed by drying the gel in an oven. First, an autoclave is separated into two parts by a membrane. The dried gel is then placed at the upper part of the autoclave (above the membrane) and it is crystallized in the presence of a little quantity of water

(or a mixture of water and structure-directing agent) placed at the bottom of the autoclave that serves as the source of vapor.

There are two forms of dry gel conversion, namely steam-assisted conversion (SAC) [100], and vapor phase transport (VPT) (Figure 2.10) [105]. In SAC method, a dried gel prepared in the presence of SDA is placed at the upper part of autoclave while pure water is put at the bottom. The heat is applied, and the crystallization is carryout and assisted by the water vapor. (Figure 2.10a). Meanwhile, The VPT method is also similar to SAC method, except the SDA is not added in the initial dry gel composition. Instead, an aqueous solution containing water and volatile SDA is used as the source of vapor placed at the bottom of the autoclave (Figure 2.10b) [100, 106]. The DGC method has advantages over the conventional hydrothermal, such as minimizing waste disposal, only a small quantity of SDA is required, reduced reactor size, synthesis of crystals of smaller size, and low pressure due to the use of very small volume of water [100, 107]. However, the main drawback of DGC method is the gaseous phase interaction with the reaction gel results in mass transfer limitation. As a result, the water and structure directing agent cannot effectively interact with the silicoaluminophosphate gel, leading to a slower rate of crystallization [108].

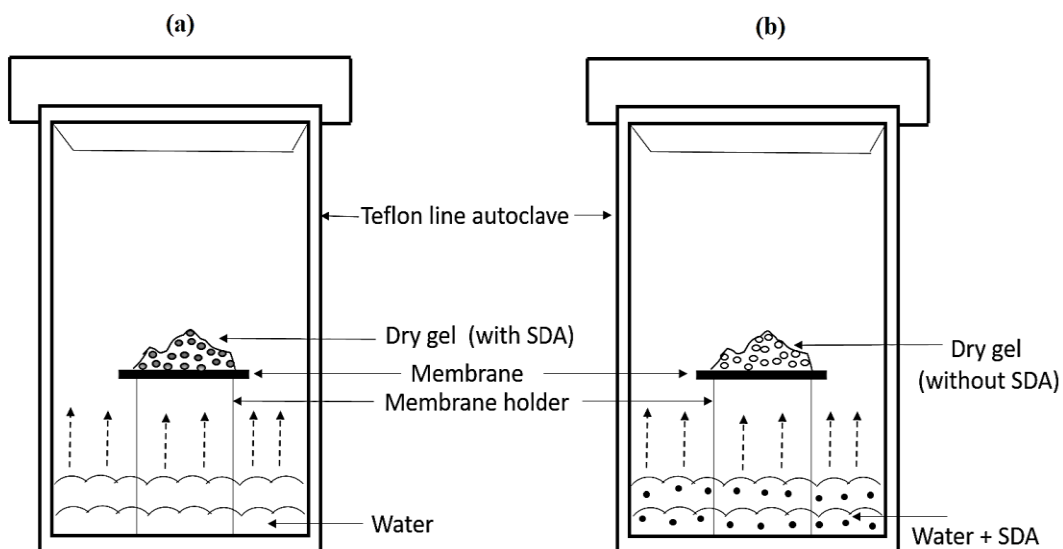


Figure 2.10 A setup for the synthesis of SAPO-5 using dry gel conversion method via (a) steam-assisted conversion (SAC) and (b) vapor phase transport (VPT) routes.

### 2.3.1(b) Microwave irradiation method

Recently, microwave synthesis has been drawing considerable attention in zeolite research [109]. This advanced heating system provides an excellent way to synthesize various zeolitic materials rapidly in a short time. Moreover, the properties of the crystalline products such as particle size distribution, morphology, crystal size and phase purity can be rationally controlled using the microwave method [109-111].

This technique is often called microwave-assisted hydrothermal synthesis because the procedure is nearly the same as classical hydrothermal heating. The basic difference between the two is the heating source. In the hydrothermal process, energy is transferred to the hydrogel by convection and conduction of heat from the material surface. On the contrary, in the microwave heating, the heat energy is generated directly from the precursor gel by molecular interactions with the microwave



electromagnetic radiation (Figure 2.11). This speed up the nucleation and crystal growth rate, and subsequently reduces the overall crystallization time from few days to merely few hours or even minutes. As a result, the reaction can proceed under homogeneous heating with minimal energy consumption [108, 112]. As such, pure phase microporous materials are produced with smaller particles and narrow size distribution [113].

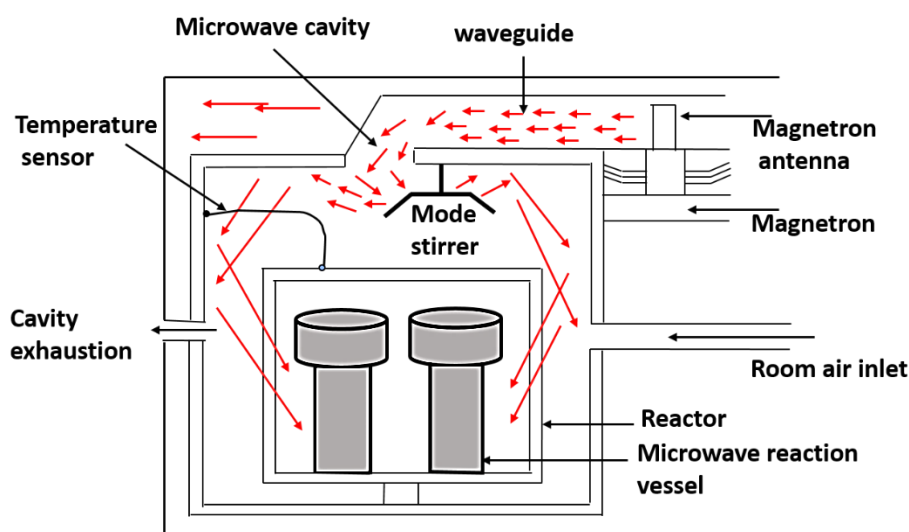


*Figure 2.11.* A diagrammatic illustration of a microwave instrument for the synthesis of microporous materials

Very recently, several researchers have successfully synthesized SAPO-5 *via* microwave heating [95, 114]. However, the major downside of microwave synthesis is that it is limited to laboratory-scale production. A large production, such as a pilot-scale above 50 L of SAPO-5 is still under investigation [112]. In contrast, the conventional hydrothermal method is still the most convenient synthesis approach for both laboratory and large-scale productions of SAPO-5 and other zeolites materials [112, 115, 116].

### 2.3.1(c) Hydrothermal synthesis

Classically, SAPO-5 is synthesized through the famous hydrothermal method where this technique was pioneered by Milton and Breck in the early 1940s [117]. The hydrothermal approach is a simple technique where a chemical reaction takes place in an aqueous medium (*hydro*) at a specific temperature above the boiling point of water (*thermal*). During the treatment, autogenic pressure is generated, and this further enhances the crystallization rate of SAPO-5 materials. During this process, water serves as a space filler and stabilizer of the porous crystal structure. Moreover, water actively facilitates the hydrolysis and reformation of T-O-T bond (T = tetrahedral atoms of Al, P or Si). Hence this enhances the chemical reaction between the precursor species and decreases the viscosity of the hydrogel.

In a typical hydrothermal synthesis of SAPO-5, the first step involves the preparation of an aqueous solution of oxides of aluminum, phosphorous, and silicon in the presence of a structure-directing agent (SDA). These solutions are mixed and stirred mechanically to obtain a homogeneous hydrogel mixture. Then, the hydrogel mixture is transferred into a Teflon lined vessel whereby it is tightly sealed in a stainless-steel autoclave (Figure 2.13). Subsequently, the reaction hydrogel is subjected to heat treatment in an electric oven for a period of few hours to a few days at a temperature range of 80-250 °C where a pressure of 1-50 bar is generated [118]. If the synthesis is performed <100 °C, polypropylene or Teflon plastic bottles can be used since no pressure is generated below the boiling temperature of water. After hydrothermal process, the crystals are separated and washed with distilled water to remove non-reacted reagents before they are oven dried.